Journal of Materials Chemistry C

Accepted Manuscript

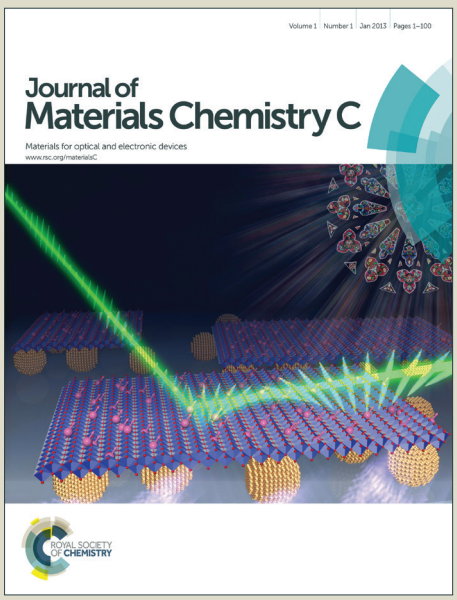

ROYAL SOCIETY OF CHEMISTRY

www.rsc.org/materialsC

Journal of Materials Chemistry C

Cite this: DOI: 10.1039/c0xx00000x

www.rsc.org/materials

PAPER

Humidity Sensor Based on Graphene/SnO_x/CFs Nanocomposites

*Tao Fu, Jian Zhu, Ming Zhuo, Bingkun Guan, Jidong Li, Zhi Xu, Bingan Lu, and Qiuhong Li**

Received (in XXX, XXX) Xth XXXXXXXXX 2013, Accepted Xth XXXXXXXXX 2013
DOI: 10.1039/c2ra00000x

In this paper, we investigated the nanocomposites composed of graphene, SnO_x and carbon fibers (CFs) for humidity sensing applications. The composites were obtained by an electrospinning method followed by adding graphene. SnO_x/CFs uniformly dispersed in graphene nanosheets. SnO_x and graphene were proved to be promising sensing materials. The amorphous carbon fibers could supply more channels for transportation of protons or electrons. Therefore, the composites exhibited high humidity sensing performance. The resistance of the sensor increases two times of magnitude with decreasing relative humidity from 55% to 30%. The sensitivity to humidity increased by almost 100% after adding graphene into SnO_x/CFs nanocomposite. The response and recovery time were 8 s and 6 s at 30% RH, respectively. The results demonstrated that rational design of nanocomposites with graphene could be a favorable strategy to improve the humidity sensing properties.

1 Introduction

The detection and control of humidity plays a very important role in our daily life and industrial fields, such as food processing, grain storage, libraries, high voltage engineering [1]. Researchers have spared no efforts to develop a humidity sensor with high sensitivity, fast response and recovery [2]. Nanostructures are considered to be excellent sensing materials for its high surface-to-volume ratio, diverse morphology and good surface and interface activity [3]. Metal oxide nanostructures have attracted great attention as sensing materials in gas and humidity sensing fields such as ZnO [4, 5], SnO_2 [6-10], In_2O_3 [11, 12]. Among these oxides, SnO_2 is a typical *n*-type semiconductor with a wide band gap (Eg=3.6 eV) at room temperature. SnO_2 possess outstanding receptivity variation in gaseous atmosphere and excellent chemical stability [6]. However, resistance-type humidity sensors based on SnO_2 usually exhibit a long response and recovery time [7,10]. The performance of these humidity sensors cannot meet the requirement of online detection. Therefore, it's necessary to develop a humidity sensor based on SnO_2 nanocomposites with enhanced performance.

Carbon nanomaterials show wonderful mechanical, electrical and chemical characteristics. Latest researches have indicated that carbon nanotubes and graphene possess remarkable properties in lithium ion batteries [13, 14], super-capacitor [15, 16], photocatalysis [17, 18] and gas sensing [19-21]. As a two-dimensional carbon nanomaterial, graphene is an ideal choice for sensing applications with large surface-to-volume ratio and stable electrical property. According to the special structure, excellent physical and chemical characters, graphene is sensitive to humidity [22-24]. Nevertheless, the sensing property of graphene was relatively weak and it needed an improvement for the practical application of high performance humidity sensors.

In our research, a composite of SnO_x nanoparticles, carbon fibers (CFs) and graphene nanosheets was designed to study its humidity sensing properties. Mesoporous SnO_2 nanotubes and SnO_x nanoparticles decorated in amorphous CFs were also obtained by electrospinning for comparison. SnO_2 nanotubes showed strong water adsorption ability and it took a long time to reach a stable state in humid atmosphere. SnO_x/CFs was found to display a faster response for humidity sensing. After graphene was added into SnO_x/CFs, the sensor showed enhanced sensitivity. Because of the special structure and their attractive physical and chemical characteristics, graphene/SnO_x/CFs (G/SnO_x/CFs) nanocomposites exhibited superior humidity sensing properties with high sensitivity, short response and recovery time.

2 Experiments

2.1 Preparation of G/SnO_x/CFs nanocomposites

All the chemicals were of analytical grade. The composite material synthesis was reported elsewhere [17]. In brief, SnO_x/CFs and SnO_2 nanotubes were synthesized by electrospinning. 0.226 g tin dichloride dehydrate ($SnCl_2 \cdot 2H_2O$, Tianjin chemical Corp., China) was dissolved in a mixed solvent of 2.2 g ethanol and 2.2 g N, N-Dimethylformamide (DMF). The obtained solution was stirred vigorously for 1 h at room temperature until it became clear. And then, 0.38 g polyvinyl pyrrolidone (PVP, sigma Aldrich, Mw≈1300000) was added in and stirred with a fast speed for 3 h. The solution was transferred into a glass syringe and a high-voltage of 20 kV was applied between the needle tip of the syringe and a bottom collector with a distance of 20 cm. Firstly,

with the facile method, as spun nanofibers were obtained. The spun fibers were collected and dried in a vacuum oven at 80 ℃ for 24 h. Then the nanofibers were annealed at 500 ℃ for 2 h with the heating rate of 3 ℃/min in argon atmosphere to prepare SnO_x/CFs. SnO_2 mesoporous tubes were obtained after annealing at 450-500 ℃ in air for comparison. Lastly, the two materials 5wt% graphene and 95wt% SnO_x/CFs were dispersed in ethanol solution with ultrasonic cell disruptor and dried at 60 □. As the solvent was fully evaporated, SnO_x/CFs was distributed in graphene networks and a uniform G/SnO_x/CFs composite was obtained.

2.2 Characterization of the material

The morphologies and microstructure of the as-synthesized samples were characterized by scanning electron microscopy (SEM, Hitachi S-4800), transmission electron microscopy (TEM) and high-resolution transmission electron microscopy (HRTEM, JEOL JEM-2100F). X-ray diffraction (XRD, Philips, X'pert pro, Cu Ka, 0.154056 nm) analysis was performed to characterize the crystal structure.

2.3 Humidity sensor fabrication and measurement

Devices with interdigital electrodes were used for humidity sensing measurement. The interdigital electrodes were fabricated by electron beam evaporation of gold on an alumina substrate and followed lift off. As shown in Fig. 1a, the strip width W of a finger was about 90 μm, and the distance between the adjacent fingers G was about 70 μm. Two leading wires were connected with the gold electrodes by soldering of tin. The as-prepared materials were dispersed in ethanol with ultrasonic cell disruptor to form a dilute paste. Then the paste was coated onto the interdigital electrodes as shown in Fig. 1b and then dried at 60 ℃ for 2 h.

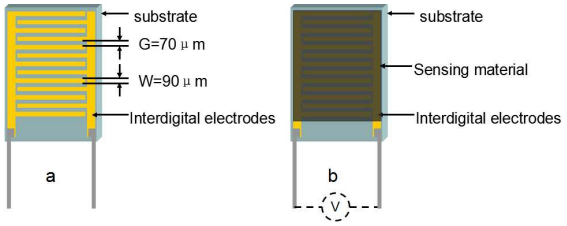

Figure 1. (a) An interdigital electrode before pasting sensing materials with the size indicated in the figure; (b) configuration of the humidity sensor.

The voltage applied between the two electrodes was 5 V. The electrical properties of the humidity sensors were measured by a high precision sensor testing system NS-4003 series (China Zhong-Ke Micro-nano IOT Ltd.). A climatic test chamber (Weiss-voetsch Environmental Testing instruments, Tai Cang Co., Ltd) supplied precisely controlled temperature and humidity. The sensor was put in the ambient atmosphere and in the control chamber with varying humidity at a constant temperature, and the real-time resistance/conductance was recorded by the sensor testing system. The atmosphere showed a humidity of 55% RH and a temperature of 20.5 ℃.

The sensitivity was defined as:

$$S = R_c/R_a \text{ (when } R_c \geq R_a)$$

Or

$$S = R_a/R_c \text{ (when } R_c \leq R_a),$$

Where R_a was the sensor resistance in the air and R_c was the resistance in the controlled chamber with adjusting humidity. In our case, a higher humidity corresponded to a smaller resistance. The response and recovery time were defined as the time it took until it achieved 90% of the total sensitivity change from one tested chamber to the other one.

3 Results and discussions

3.1 Morphologies of the materials

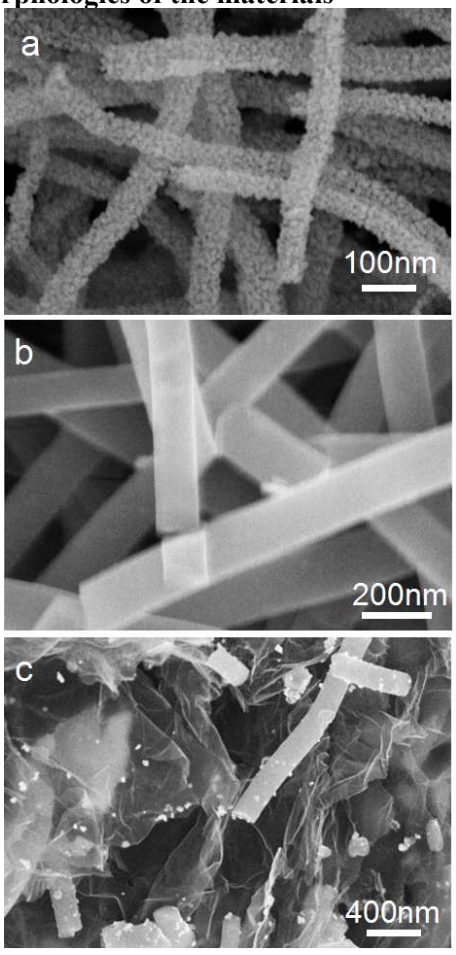

Figure 2. SEM images of the (a) SnO_2 mesoporous nanotubes, (b) SnO_x/CFs, and (c) G/SnO_x/CFs nanocomposite.

The morphologies of the as-synthesized fibers were shown in Fig. 2a-c. In a typical electrospinning process, the $SnCl_2$ mixture droplet at the needle tip of the syringe would be distorted into a conical sharp by high external voltage static electric field. When the static electric field is strong enough, charges on the droplet will overcome the surface tension to form a liquid jet. The liquid jet was accelerated toward the collector because of static

electric force. Then, the fibers were obtained [26]. With different annealing conditions, the electrospun fibers resulted in varied morphologies and components. As shown in Fig. 2a, the diameter of nanotubes was 50-100 nm. The surface of the tubes was rough and consisted of lots of nanoparticles after annealing in air, because PVP decomposed into gas at high temperature in air and numerous nanograins was left and formed continuous porous SnO_2 tubes. As for the one annealed in an inert environment, PVP acted as a precursor of carbon fibers, and SnO_x nanoparticles distributed in carbon. From Fig. 2b, the average diameter of SnO_x/CFs was about 120 nm. As can be seen in Fig. 2c, the SnO_x/CFs were uniformly dispersed in graphene and many SnO_x nanoparticles distributed on the surface of amorphous carbon fibers.

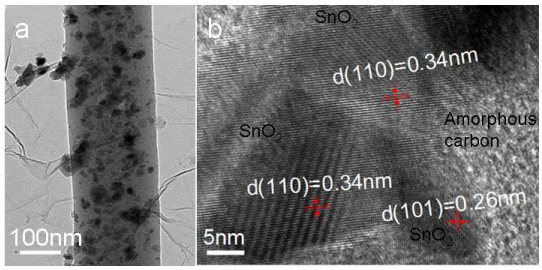

Figure 3. (a) TEM image of G/SnO_x/CFs, (b) High resolution TEM image of G/SnO_x/CFs

The materials were characterized by XRD and the results demonstrated that rutile phase SnO_2 was obtained for the case of annealing in air (Fig. S1). For the composite of G/SnO_x/CFs, XRD peaks corresponding to SnO_2 and Sn_3O_4 were observed, mightily due to partially reduced Sn^{4+} by carbon. No obvious carbon peaks were found in XRD results, possibly due to the formation of amorphous carbon fibers, which were verified in HRTEM results. Figure 3a was the typical TEM image of G/SnO_x/CFs at a low magnification. Apparently, SnO_x nanoparticles were dispersed in the nanofibers of amorphous carbon. Fig. 3b shows HRTEM image of G/SnO_x/CFs. A lattice spacing of 0.26 nm and 0.34 nm was observed, corresponding to the (101) and (110) planes of rutile phase SnO_2 (JCPDS NO. 41-1445), respectively.

3.2 Humidity sensing properties

3.2.1 Humidity sensing response

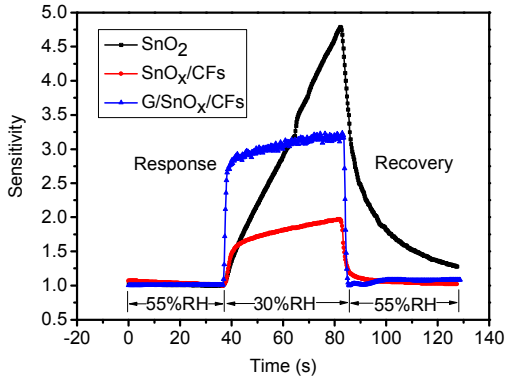

Figure 4. Time-dependent response and recovery curve of the three samples as the relative humidity was changed between 55% and 30%.

Fig. 4 shows humidity response of the sensors based on SnO_2 nanotubes, SnO_x/CFs and G/SnO_x/CFs nanocomposites as the relative humidity switching between 55% and 30% at 20.5℃. Obviously, the SnO_2 nanotubes could reach the highest sensitivity compared with the other two sensors. But it took a very long time to reach a stable value, demonstrating a long response and recovery time for SnO_2 sensor. In contrast, the response and recovery time of SnO_x/CFs were much shorter, which were 10 s and 8 s, respectively. The sensitivity was about 1.86 as the humidity was varied from 55 to 30% RH. G/SnO_x/CFs sensor showed a shorter response and recovery time of 8 s and 6 s, respectively. And the sensitivity of G/SnO_x/CFs sensor was about 3.35, almost twice over SnO_x/CFs sensor.

3.2.2 Dynamic response and recovery.

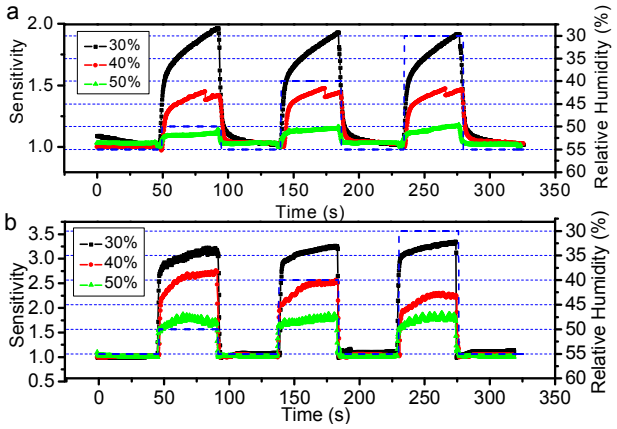

Figure 5. Dynamic response of (a) : SnO_x/CFs and (b) : G/SnO_x/CFs as the relative humidity was changed from ambient air to controlled one.

The dynamic response and recovery property was tested under a series of switches between atmosphere humidity (55%) and different controlled ones (30% - 80%) with a step of 10%RH at 20.5 ℃. Fig. 5 shows the response of the two sensors between ambient relative humidity (55%) and test humidity from 30% to 50%. During the three cycles at different humidity, the sensor showed repeatable response. As shown in Fig. 5, the G/SnO_x/CFs sensor displays a higher sensitivity compared with SnO_x/CFs. The curves also demonstrate that G/SnO_x/CFs sensor takes a shorter response and recovery time.

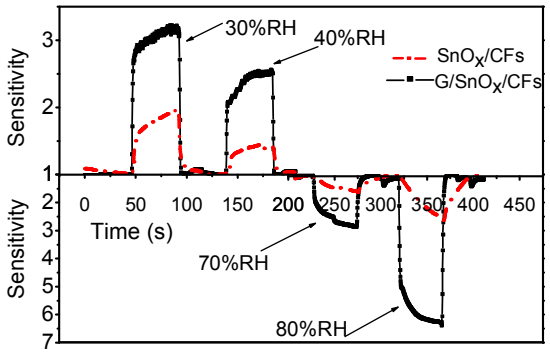

Figure 6. The response at different humidity levels of the two sensors.

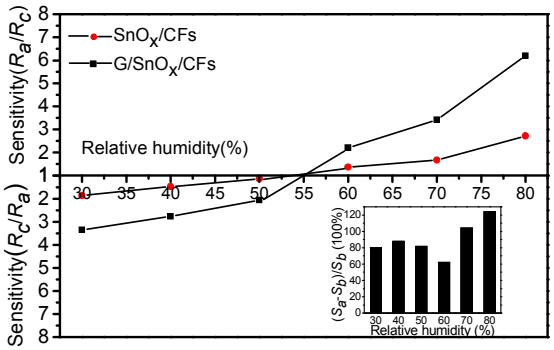

Figure 7. Sensitivity of the two sensors with the relative humidity ranging from 30% to 80%. The insert is the sensitivity difference of SnO_x/CFs and G/SnO_x/CFs. S_b (sensitivity before added graphene) and S_a (sensitivity after added graphene) are the sensitivity of SnO_x/CFs and G/SnO_x/CFs, respectively.

Sensitivity is an important parameter for a sensing device. Fig. 6 is the dynamic response of the two sensors switching between 30%, 40%, 70%, 80% and 55%. Fig. 7 shows the sensitivity at different RHs. The sensitivity of G/SnO_x/CFs was calculated to be 3.35, 2.76, 2.05, 2.2, 3.41, and 6.2 as the sensitivity was changed from 55% to 30, 40, 50, 60, 70, and 80%, respectively. Obviously, the sensitivity of G/SnO_x/CFs is higher than SnO_x/CFs at each relative humidity. The insert in Fig. 7 shows the difference of sensitivity for two sensors. The sensitivity after adding graphene into SnO_x/CFs had been enhanced about 60-120%, indicating that graphene could improve the humidity sensing performance.

3.3 Discussion

SnO_2 was known to be a perfect sensing material. In our work, the SnO_2 nanotubes also showed a high sensitivity to water vapor. However, it took several minutes to reach a relatively stable state as shown in Fig. 4. As seen in Fig. 2b, c and Fig. 3a, SnO_x nanoparticles dispersed in amorphous carbon nanofibers. On one hand, this structure reduced the action area of SnO_x with water vapor; on the other hand, the amorphous CFs could supply more channels for charge carriers. Amorphous carbon was reported to be an effective protective layer against water molecules for a short time (less than 2 h) exposed to a high humidity (100% RH) at room temperature [27]. So the sensitivity of SnO_x/CFs was most related to SnO_x nanoparticles on the surface of amorphous carbon nanofibers. The sensitivity of SnO_x/CFs was lower compared with pure SnO_2, but the response and recovery time was much shorter.

Several mechanisms have been suggested to explain the humidity sensing property for SnO_2. The conductivity of humidity sensor can be varied due to either adsorption of the water on the surface, or the replacement of oxygen by water molecules [28, 29]. Moreover, oxygen vacancies act as active sites to promote the adsorbed water molecules dissociation [30]. Density functional theory calculations proved that water dissociation probably only took place at oxygen vacancies [30].

Fig. 8 shows the stages of water molecules dissociation and further adsorption of water by hydrogen bond. When the material is exposed to a higher humidity, the pre-adsorbed oxygen is replaced by water molecules and releases electron at the same time. Water molecules adsorbed on grain surface and react with lattices oxygen, as

$$H_2O + O_o + 2Sn \leftrightarrow 2OH\text{-}Sn + V_o^{2+} + 2e^-$$

Here, O_o is lattice oxygen and V_o the oxygen vacancy [31]. SnO_x layers consist of nanosized polycrystalline phase of SnO_2, Sn_2O_3, Sn_3O_4 and TeO_2 are sensitive humidity and ethanol sensor [32]. The SnO_x/CFs nanocomposites were obtained after calcination and oxygen vacancies left which can act as active sites for water adsorption [33]. It has been reported that both water molecules and hydroxyl groups are able to dissociate, supplying mobile protons [34]. At a high humidity level, more water is adsorbed via hydrogen bond and forms a continuous water film. At this time, protons act as major charge carries which can transport in the adsorbed water. As the ambient humidity increases, the amount of water molecules on the surface of sensor increases, and enhances the concentration of H^+ or H_3O^+ which raises the conductivity of the humidity sensor.

It was reported that water molecules adsorbed on graphene would form many water clusters by hydrogen bond, and for the water cluster, the cluster link usually was a donor [35]. Therefore, water molecule adsorption on graphene could increase the conductance of the G/SnO_x/CFs composite. In the moisture atmosphere, more and more water molecules can adsorbed on to the water cluster by hydrogen bond. Graphene owes huge specific surface area which can adsorb large amount of water molecules which enhances the adsorption capability of the composite. Benefiting from the special structure of G/SnO_x/CFs nanocomposites, water molecules adsorbed on graphene can transfer to SnO_x which leading to a higher sensitivity and quicker response for the nanocomposites. Therefore, graphene is beneficial to enhancing the humidity performance of our composite.

Although capacitive-type humidity sensors based on SnO_2 or graphene oxide films exhibited very high sensitivity and fast response [8, 36], humidity sensors with direct current (DC) measurement based on SnO_2 or graphene films usually showed lower sensitivity or slower response [23, 24, 37]. The SnO_2 film displayed sensitivity about 2.5 with RH changing from 40 to 90% [37]. The graphene sensitivity was about 0.73 with humidity changing from 3% to 30%, and the response time was as long as 50 s [23]. Our sensor based on SnO_2-nanotube film displayed an unsaturated response to humidity with sensitivity higher than 4.7 and long-time response. Moreover, sensors based on G/SnO_x/CFs film showed a sensitivity of 6.22 as the sensitivity was changed from 55% to 80% with the response time about 6-8 s, demonstrating the synergetic effect of graphene and SnO_2.

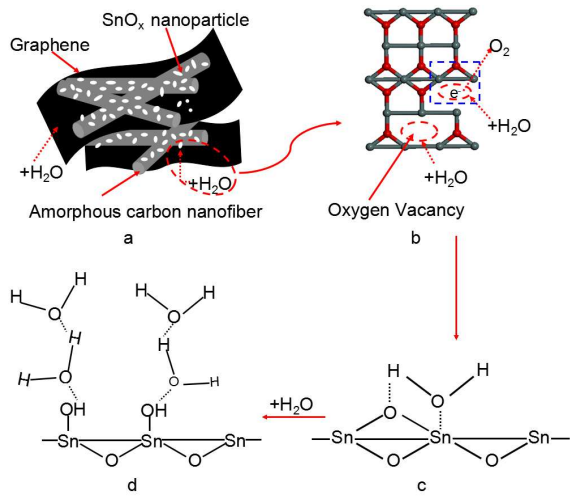

Figure 8. (a) The morphology and structure of G/SnO_x/CFs. (b) Ball-and-stick model of water molecules dissociate on oxygen vacancies. (c) Oxygen vacancy acts as active site to promote water molecule dissociated. (d) Hydroxyl groups were formed and further adsorption of water molecules through bridging hydrogen bond. Red atoms: O; Grey atoms: Sn.

4 Conclusions

In summary, we have synthesized a nanocomposite of G/SnO_x/CFs and investigated its humidity sensing properties. For comparison, pure SnO_2 mesoporous tubes and SnO_x/CFs based humidity sensors are also fabricated. The humidity sensing test results demonstrated that graphene was quite useful to improve the sensor performance. The response and recovery time was shortened from several minutes to 6-8 s. Compared with SnO_x/CFs sensors, the sensitivity of G/SnO_x/CFs has been greatly improved from 2.71 to 6.22, with the relative humidity switched from 55 to 80% RH. All the study indicates that the composite with graphene is promising for fabricating humidity sensors with advanced properties.

Acknowledgements

This work was partly supported by the financial support of the National Natural Science Foundation of China (Grant No. 21003041, 61376073), and the Specialized Research Fund for the Doctoral Program of Higher Education of China (Grant No. 20120161110016).

References

1 R Nohria, R K Khillan, Y Su, R Dikshit, Y Lvov and K Varahramyan, *Sensors and Actuators B: Chemical,* 2006, **114**, 218-222.
2 Y Yao, X Chen, H Guo, Z Wu and X Li, *Sensors and Actuators B: Chemical,* 2012, **161**, 1053-1058.
3 X M Yin, C C Li, M Zhang, Q Y Hao, S Liu, Q H Li, L B Chen and T H Wang, *Nanotechnology,* 2009, **20**, 455503.
4 L M Li, Z F Du and T H Wang, *Sensors and Actuators B: Chemical,* 2010, **147**, 165-169.
5 Q Qi, T Zhang, Q J Yu, R Wang, Y Zeng, L Liu, H B Yang, *Sensors and Actuators B: Chemical,* 2008, **133**, 638-643.
6 Q Kuang, C S Lao, Z L Wang, Z X Xie and L S Zheng, *Journal of the American Chemical Society,* 2007, **129**, 6070-6071.
7 M Parthibavarman, V Hariharan and C Sekar, *Materials Science and Engineering: C,* 2011, **31**, 840-844.
8 X F Song, Q Qi, T Zhang and C Wang, *Sensors and Actuators B: Chemical,* 2009, **138**, 368-373.
9 B Wang, L F Zhu, Y H Yang, N S Xu and G W Yang, *Journal of Physical Chemistry C*, 2008, **112**, 6643-6647.
10 L J Li, K Yu, J Wu, Y Wang and Z Q Zhu, *Crystal Research and Technology*, 2010, **45**, 539-544.
11 X W Liu, R Wang,T Zhang, Y He, J C Tu, X T Li, *Sensors and Actuators B: Chemical,* 2010, **150**, 442-448.
12 Q C Liang, H L Xu, J X Zhao, S Gao, *Sensors and Actuators B: Chemical,* 2012, **165**, 76-81.
13 S H Ng, J Wang, Z P Guo, J Chen, G X Wang and H K Liu, *Electrochimica Acta*, 2005, **51**, 23-28.
14 B J Landi, M J Ganter, C D Cress, R A Dileo and R P Raffaelle, *Energy & Environment Science*, 2009, 2, 638-654.
15 J Sun and H Bi, *Materials Letters*, 2012, **81**, 48-51.
16 Y Li, N Q Zhao, C S Shi, E Z Liu and C N He, *Journal of Physical Chemistry C*, 2012, **116**, 25226 25232.
17 Q J Xiang, J g Yu and M Jaroniec, *Chemical Society Reviews*, 2012, **41**, 782-796.
18 G Williams, B Seger and P V Kamat, *ACS Nano*, 2008, 2, 1487-1491.
19 F Schedin, A K Geim, S V morozov, E W Hill, P Blake, M I Katsnelson and K S Novoselov, *Nature Materials*, 2007, 6, 652-655.
20 H Y Jeong, D S Lee, H K Choi, D H Lee, J E Kim, J Y Lee, W J Lee, S O Kim and S Y Choi, *Applied Physics Letters,* 2010, **96**, 213105.
21 U Lange, T Hirsch, V M. Mirsky, O S. Wolfbeis, *Electrochimica Acta,* 2011, **56**, 3707-3712.
22 J L Zhang, G X Shen, W J Wang, X J Zhou and S W Guo, *Journal of Materials Chemistry,* 2010, **20**, 10824-10828.
23 Q W Huang, D W Zeng, S Q Tian and C S Xie, *Materials Letters,* 2012, **83**, 76-79.
24 A Ghosh , D J Late , L S Panchakarla, A Govindaraj and C N R Rao, *Journal of Experimental Nanoscience,* 2009, **4**, 313-322.
25 J Zhu, D N Lei, G H Zhang, Q H Li, B A Lu and T H Wang, *Nanoscale*, 2013, **5**, 5499-5505.
26 Z M Huang, Y Z Zhang, M kotaki and S Ramakrishna, *Composites Science and Technology*, 2003, 63, 2223-2253.
27 S Tsuchitani, Y Sogawa, R Kaneko, S Hirono and S Umemura, *Wear,* 2003, **254**, 1042-1049.
28 W Wang, Z Y Li, L Liu, H N Zhang, W Zheng, Y Wang, H M Huang, Z J Wang and C Wang, *Sensors and Actuators B: Chemical,* 2009, **141**, 404-409.
29 Y S Zhang, Yu K, D S Jiang, Z Q Zhu, H R Geng and L Q Luo, *Applied Surface Science,* 2005, **242**, 212-217.
30 R Schaub, P Thostrup, N Lopez, E Lægsgaard, I Stensgaard, J K Nørskov and F Besenbacher, *Physical Review Letters,* 2001, **87**, 2066104-1-2066104-4.
31 N K Pandey, K Tiwari and Akash Roy, *Bull. Mater. Sci.*, 2012, **3**, 347-352.
32 B Georgieva, D Nihtianova, J Pirov and I Podolesheva, *Journal of Physics: Conference Series*, 2010, 223, 012018.

33 O M Berengue, R A Simon, A J Chiquito, C J Dalmaschio, E R Leite, H A Guerreiro and F E G Guimarães, *Journal of Applied Physics*, 2010,**107**, 033717.
34 J H Anderson and G A Parks, *Journal* of *Physical Chemistry,* 1968, **72**, 10, 3662-3668.
35 J Berashevich and T Chakraborty, *Physical Review B*, 2009, **80**, 033404.
36 H C Bi, K B Yin, X Xie, J Jin, S Wan, L T Sun, M Terrones and M S Dresselhaus, *Scientific Reports*, 2013, **3**, 1-7.
37 N D Md Sin, S Ahmad, M F Malek, M H Mamat and Rusop, *IOP Conf.Series: Materials Science and Engineering*, 2013, **46**, 1-7.

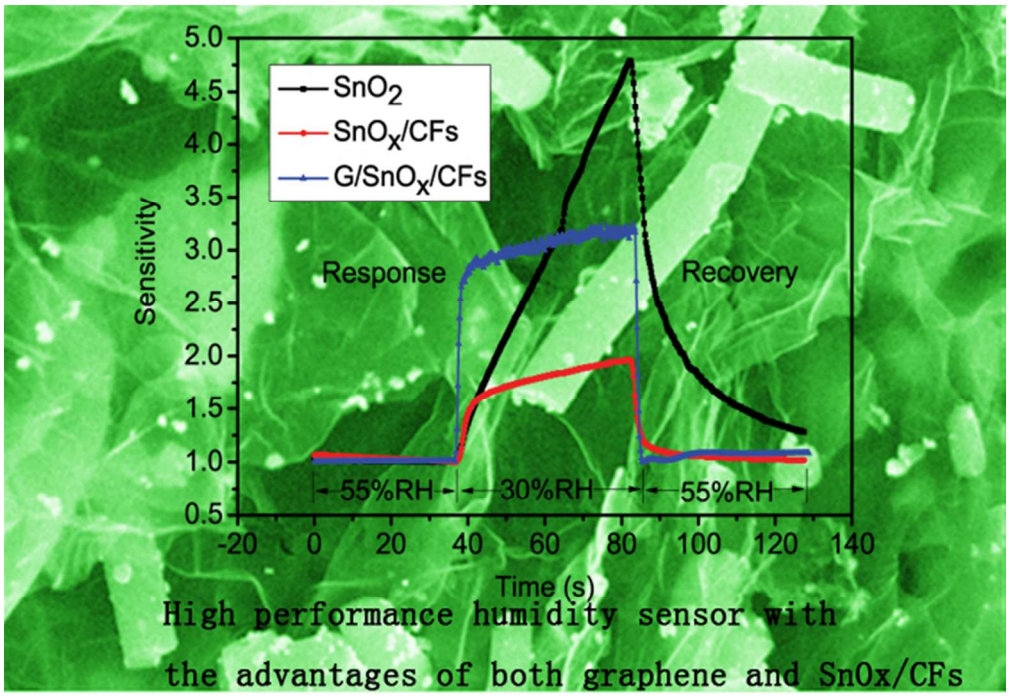

184x126mm (96 x 96 DPI)